Layerwise electro-elastic user-defined elements in Abaqus for static and free vibration analysis of piezoelectric composite plates

João Pedro Dos Anjos Moreira
joao.anjos.moreira@tecnico.ulisboa.pt

Instituto Superior Técnico, Universidade de Lisboa, Portugal

January 2021

Abstract

The development of reliable methods for analysis of piezoelectric multilayered composite structures is motivated by a wide range of applications in aerospace engineering, combining high specific mechanical properties of composite materials, with monitoring and actuation capabilities of the piezoelectric materials. Consequently, this work presents a computational study in static and free vibration analysis, using two electro-elastic plate elements implemented in a user-defined element (UEL) subroutine available in Abaqus. On both of them, a Layerwise description for three discrete layers is used, assuming in each layer a first-order shear deformation displacement field, as well as a linear or quadratic z-expansion of the electric potential, respectively, UEL1 and UEL2. Furthermore, the models here developed are compared with three-dimensional exact solutions, available for the case of simply-supported plates reported in the literature. Two multilayered plates with different piezoelectric materials in the face layers are considered, from the case of thin, moderately thick to thick plates. The models predictive capabilities in static response for the displacements, electric potential and in-plane stresses is demonstrated to be in agreement with the exact solutions for thin and moderately thick plates. In free vibration analysis, the first twelve vibration modes and frequencies predicted by the developed models, reveal a good accuracy of the models comparatively to the exact solutions, even for thicker plates.

Keywords: Piezoelectric composite plates, Abaqus user-defined element, Layerwise theory, First-order theory, Electro-elastic modelling

1. Introduction

The development of reliable methods for analysis of piezoelectric multilayered composite structures is motivated by a wide rage of engineering applications, combining high specific mechanical properties of composite materials, with monitoring and actuation capabilities of the piezoelectric materials. In fact, when a multilayered composite plate with skin layers made of transversely poled actuators (extension mode) is subjected to an applied transverse electric field, the piezoelectric layers undergo in-plane deformations, where the lateral dimensions are increased or decreased, forcing the remaining substrate elastic layers in the multilayered composite core to deform. This work presents a computational study in static and free vibration analysis, using two electro-elastic plate elements implemented with user-defined element (UEL) subroutine available in Abaqus, taking advantage of the mesh generation, assembly procedures, application of boundary conditions and loads, as well as the robust numerical solvers and the visualization features.

By the 90's, Heyliger [1] solved static and dynamic three-dimensional (3D) equilibrium electro-elastic equations for simply-supported piezoelectric multilayered composite plates, considering the case of transversely poled piezoelectric orthotropic layers. A zig-zag through-thickness continuous displacement field and electric potential is demonstrated, as well as continuous transverse stresses and transverse electric displacement in the absence of internal electrodes, leading to the commonly known C_z^0 interlaminar continuity conditions. In-plane stresses and in-plane electric displacements are typically discontinuous between adjacent layers due to a possible change of the mechanical and electrical properties along the stacking scheme. More recently, electro-elastic exact solutions for static and free vibration analysis of piezoelectric multilayered composite plates are reported by Moleiro et al. [2].

Attempting to build an efficient electro-elastic element, for analysis of piezoelectric composite plates with low computational effort, the present work focus on bi-dimensional plate elements, based on a classical axiomatic discrete Layerwise (LW)

model, for three discrete layers, that fulfills the C_z^0-requirements for the primary variables: displacements and electric potential. The model assumes a multilayered composite core treated with an Equivalent Single Layer (ESL) Theory, with piezoelectric face layers on both top and bottom surfaces.

Following two remarkable works, Reddy's book [3] and Carrera [4], each discrete layer is treated individually, where the assumed First-Order Shear Deformation Theory (FSDT) displacement field is modified to account for the interlaminar continuity conditions. For the LW electric potential, a linear z-expansion is used in UEL1, while a quadratic one is used in UEL2 to enhance the electromechanical coupling, as suggested in Benjeddou [5].

2. Fundamental Electro-Elastic Equations

The theory of electroelasticity relies on the governing equations of motion of elastic bodies and electric charge conservation of dielectrics, where for piezoelectric materials both equations are coupled through the constitutive law, as explained in Reddy [3]. The equilibrium equations in terms of the stress tensor components σ_{ij} and the displacement components u_i, for $i,j = \{1,2,3\}$, with $(u_1,u_2,u_3) \equiv (u,v,w)$, in the absence of body forces are:

$$\sigma_{ij,j} = \rho \ddot{u}_i \tag{1}$$

where ρ is the material density and, for conciseness, the comma notation is used to represent the partial derivative, as well as the double dot to denote the second time derivative.

The charge equation of electrostatics, in the absence of electric body charges, is given in terms of the electric displacement components D_i, with $i = \{1,2,3\}$ as follows:

$$D_{i,i} = 0 \tag{2}$$

For small displacements, the strain-displacement relation follows the definition of the infinitesimal strain tensor ε_{ij} as shown:

$$\varepsilon_{ij} = \left(u_{i,j} + u_{j,i}\right)/2 \tag{3}$$

where for $i \neq j$, the engineering shear strains are given as $\gamma_{ij} = 2\varepsilon_{ij}$.

Under the electro-quasi-static assumption, the electric field is irrotational, being the field-potential relation given by:

$$E_i = -\phi_{,i} \tag{4}$$

where E_i is the electric field components and ϕ the electric potential.

The piezoelectric constitutive equations, using a single-index notation for the stress and strain tensors, holds:

$$\sigma_i = C_{ij}\varepsilon_j - e_{ik}E_k \tag{5a}$$

$$D_k = e_{kj}\varepsilon_j + \epsilon_{kl}E_l \tag{5b}$$

where $i,j = \{1,..,6\}$ and $k,l = \{1,2,3\}$, noting that for $k = l$ and $j = \{1,2,3\}$ results $\varepsilon_j = \varepsilon_{kl}$, as well as for $k \neq l$ and $j = \{4,5,6\}$ results $\varepsilon_j = 2\varepsilon_{kl} = \gamma_{kl}$. Also, C_{ij} are the elastic coefficients, e_{ik} the piezoelectric coefficients and ϵ_{kl} the dielectric coefficients.

Assuming a plane stress state ($\sigma_3 = \sigma_{33} = 0$), the transversely poled piezoelectric constitutive equations in the material coordinate system (x_1,x_2,x_3) become,

$$\begin{Bmatrix}\sigma_{11}\\ \sigma_{22}\\ \sigma_{23}\\ \sigma_{13}\\ \sigma_{12}\end{Bmatrix} = \begin{bmatrix}Q_{11} & Q_{12} & 0 & 0 & 0\\ Q_{12} & Q_{22} & 0 & 0 & 0\\ 0 & 0 & Q_{44} & 0 & 0\\ 0 & 0 & 0 & Q_{55} & 0\\ 0 & 0 & 0 & 0 & Q_{66}\end{bmatrix}\begin{Bmatrix}\varepsilon_{11}\\ \varepsilon_{22}\\ \gamma_{23}\\ \gamma_{13}\\ \gamma_{12}\end{Bmatrix} - \begin{bmatrix}0 & 0 & e_{31}^*\\ 0 & 0 & e_{32}^*\\ 0 & e_{24} & 0\\ e_{15} & 0 & 0\\ 0 & 0 & 0\end{bmatrix}\begin{Bmatrix}E_1\\ E_2\\ E_3\end{Bmatrix} \tag{6a}$$

$$\begin{Bmatrix}D_1\\ D_2\\ D_3\end{Bmatrix} = \begin{bmatrix}0 & 0 & 0 & e_{15} & 0\\ 0 & 0 & e_{24} & 0 & 0\\ e_{31}^* & e_{32}^* & 0 & 0 & 0\end{bmatrix}\begin{Bmatrix}\varepsilon_{11}\\ \varepsilon_{22}\\ \gamma_{23}\\ \gamma_{13}\\ \gamma_{12}\end{Bmatrix} + \begin{bmatrix}\epsilon_{11} & 0 & 0\\ 0 & \epsilon_{22} & 0\\ 0 & 0 & \epsilon_{33}^*\end{bmatrix}\begin{Bmatrix}E_1\\ E_2\\ E_3\end{Bmatrix} \tag{6b}$$

where the new material properties are reduced plane stress elastic constants Q_{ij}, reduced piezoelectric coefficients e_{ij}^* and reduced dielectric constants ϵ_{ij}^* are obtained as follows:

$$Q_{ij} = C_{ij} - C_{i3}C_{j3}/C_{33}, \quad i,j = \{1,2\} \tag{7a}$$

$$Q_{44} = C_{44}\ ,\ Q_{55} = C_{55}\ ,\ Q_{66} = C_{66} \tag{7b}$$

$$e_{3i}^* = e_{3i} - e_{33}C_{i3}/C_{33}, \quad i,j = \{1,2\} \tag{7c}$$

$$\epsilon_{33}^* = \epsilon_{33} + e_{33}^2/C_{33} \tag{7d}$$

In order to use the global coordinate system (x,y,z) basis, a rotation on the x-y plane must be applied to the constitutive matrices in order to obtain the piezoelectric constitutive law as shown:

$$\begin{Bmatrix}\sigma_{xx}\\ \sigma_{yy}\\ \tau_{yz}\\ \tau_{xz}\\ \tau_{xy}\end{Bmatrix} = \begin{bmatrix}\bar{Q}_{11} & \bar{Q}_{12} & 0 & 0 & \bar{Q}_{16}\\ \bar{Q}_{12} & \bar{Q}_{22} & 0 & 0 & \bar{Q}_{26}\\ 0 & 0 & \bar{Q}_{44} & \bar{Q}_{45} & 0\\ 0 & 0 & \bar{Q}_{45} & \bar{Q}_{55} & 0\\ \bar{Q}_{16} & \bar{Q}_{26} & 0 & 0 & \bar{Q}_{66}\end{bmatrix}\begin{Bmatrix}\varepsilon_{xx}\\ \varepsilon_{yy}\\ \gamma_{yz}\\ \gamma_{xz}\\ \gamma_{xy}\end{Bmatrix} - \begin{bmatrix}0 & 0 & \bar{e}_{31}\\ 0 & 0 & \bar{e}_{32}\\ \bar{e}_{14} & \bar{e}_{24} & 0\\ \bar{e}_{15} & \bar{e}_{25} & 0\\ 0 & 0 & \bar{e}_{36}\end{bmatrix}\begin{Bmatrix}E_x\\ E_y\\ E_z\end{Bmatrix} \tag{8a}$$

$$\begin{Bmatrix}D_x\\ D_y\\ D_z\end{Bmatrix} = \begin{bmatrix}0 & 0 & \bar{e}_{14} & \bar{e}_{15} & 0\\ 0 & 0 & \bar{e}_{24} & \bar{e}_{25} & 0\\ \bar{e}_{31} & \bar{e}_{32} & 0 & 0 & \bar{e}_{36}\end{bmatrix}\begin{Bmatrix}\varepsilon_{xx}\\ \varepsilon_{yy}\\ \gamma_{yz}\\ \gamma_{xz}\\ \gamma_{xy}\end{Bmatrix} + \begin{bmatrix}\epsilon_{xx} & \epsilon_{xy} & 0\\ \epsilon_{xy} & \epsilon_{yy} & 0\\ 0 & 0 & \epsilon_{zz}\end{bmatrix}\begin{Bmatrix}E_x\\ E_y\\ E_z\end{Bmatrix} \tag{8b}$$

where the transformed properties are derived in Reddy [3]. Using compact invariant notation, equation (8) turns:

$$\{\sigma\} = \left[\bar{Q}\right]\{\varepsilon\} - [\bar{e}]\{E\} \tag{9a}$$

$$\{D\} = [\bar{e}]^T\{\varepsilon\} + [\bar{\epsilon}]\{E\} \tag{9b}$$

3. Layerwise Model

The layerwise displacement field is developed for a model with three discrete layers, driven by the assumption of a multilayered composite plate treated

with ESL theory, with piezoelectric face layers, where no slip occurs at the interfaces between layers, represented in figure 1. The composite core (c) is modelled with a first-order theory, as well as the piezoelectric top (t) and bottom (b) layers. Also, both linear and quadratic z-expansions for the electric potential are considered for each discrete layer.

3.1. Displacement Field

Following the assumed stacking sequence $[t/c/b]$, the FSDT displacement field for the discrete layers holds,

$$\begin{aligned} u_c(x,y,z,t) &= u_{0_c}(x,y,t) + z\theta_{x_c}(x,y,t) \\ v_c(x,y,z,t) &= v_{0_c}(x,y,t) + z\theta_{y_c}(x,y,t) \\ w_c(x,y,z,t) &= w_{0_c}(x,y,t) \end{aligned} \tag{10}$$

$$\begin{aligned} u_t(x,y,z,t) &= u_{0_t}(x,y,t) + (z-\bar{z}_t)\theta_{x_t}(x,y,t) \\ v_t(x,y,z,t) &= v_{0_t}(x,y,t) + (z-\bar{z}_t)\theta_{y_t}(x,y,t) \\ w_t(x,y,z,t) &= w_{0_t}(x,y,t) \end{aligned} \tag{11}$$

$$\begin{aligned} u_b(x,y,z,t) &= u_{0_b}(x,y,t) + (z-\bar{z}_b)\theta_{x_b}(x,y,t) \\ v_b(x,y,z,t) &= v_{0_b}(x,y,t) + (z-\bar{z}_b)\theta_{y_b}(x,y,t) \\ w_b(x,y,z,t) &= w_{0_b}(x,y,t) \end{aligned} \tag{12}$$

where the generalized displacements $u_{0_{(k)}}$, $v_{0_{(k)}}$ and $w_{0_{(k)}}$ are the displacement components for the mid-plane of the k-layer, $\theta_{x_{(k)}}$ and $\theta_{y_{(k)}}$ the associated rotations about the y-axes (anticlockwise) and x-axes (clockwise), respectively, and $\bar{z}_t$ and $\bar{z}_b$ are the mid-plane transverse coordinates for both top and bottom layers, respectively, obtained from figure 1 as follows:

$$\bar{z}_t = (h_c + h_t)/2 \ , \ \bar{z}_b = -(h_c + h_b)/2 \tag{13}$$

In order to fulfill the C_z^0-requirements for the displacements, the interlaminar continuity conditions must be verified for all displacement components. Since the FSDT transverse displacement is assumed to be independent on the z-coordinate, the interlaminar continuity conditions for the transverse displacement leads to,

$$w_c(x,y,t) = w_t(x,y,t) = w_b(x,y,t) = w_0(x,y,t) \tag{14}$$

where w_0 represents the plate's mid-plane ($z = 0$) transverse displacement. The continuity conditions for the in-plane displacements at the interfaces between the piezoelectric face layers and the composite core as follows,

$$u_c\left(x,y,h_c/2,t\right) = u_t\left(x,y,\bar{z}_t - h_t/2,t\right) \tag{15a}$$
$$v_c\left(x,y,h_c/2,t\right) = v_t\left(x,y,\bar{z}_t - h_t/2,t\right) \tag{15b}$$
$$u_c\left(x,y,-h_c/2,t\right) = u_b\left(x,y,\bar{z}_b + h_b/2,t\right) \tag{15c}$$
$$v_c\left(x,y,-h_c/2,t\right) = v_b\left(x,y,\bar{z}_b + h_b/2,t\right) \tag{15d}$$

allow to reduce the number of unknowns in equations (10) to (12), when writing the rotations of both bottom and top layers, $(\theta_{x_b}, \theta_{y_b})$ and $(\theta_{x_t}, \theta_{y_t})$, respectively, as a function of the remaining unknowns.

Solving the continuity conditions (15) for the displacements defined in equations (10) to (12), one obtains the LW-FSDT in-plane displacements for the piezoelectric face layers as follows,

$$u_t = u_{0_t} + (z-\bar{z}_t)\left(\alpha_1 u_{0_c} + \alpha_2\theta_{x_c} + \alpha_3 u_{0_t}\right) \tag{16a}$$
$$v_t = v_{0_t} + (z-\bar{z}_t)\left(\alpha_1 v_{0_c} + \alpha_2\theta_{y_c} + \alpha_3 v_{0_t}\right) \tag{16b}$$
$$u_b = u_{0_b} + (z-\bar{z}_b)\left(\beta_1 u_{0_c} + \beta_2\theta_{x_c} + \beta_3 u_{0_b}\right) \tag{16c}$$
$$v_t = v_{0_b} + (z-\bar{z}_b)\left(\beta_1 v_{0_c} + \beta_2\theta_{y_c} + \beta_3 v_{0_b}\right) \tag{16d}$$

where the layerwise constants α_k and β_k are:

$$\alpha_1 = -2/h_t, \ \alpha_2 = -h_c/h_t, \ \alpha_3 = -\alpha_1 \tag{17a}$$
$$\beta_1 = 2/h_b, \ \beta_2 = -h_c/h_b, \ \beta_3 = -\beta_1 \tag{17b}$$

The relation between the displacement components for each k-discrete layer, for $k = \{c,t,b\}$, and the nine independent mechanical unknowns, ordained in the vector of mechanical degrees of freedom (DOFs) $\{d\}$ defined as shown,

$$\{d\} = \{u_{0_c} \ v_{0_c} \ w_0 \ \theta_{x_c} \ \theta_{y_c} \ u_{0_t} \ v_{0_t} \ u_{0_b} \ v_{0_b}\}^T \tag{18}$$

is achieved through a matrix $[Z]_{(k)}$ which gives,

$$\{u\}_{(k)} = \{u_{(k)} \ v_{(k)} \ w_{(k)}\}^T = [Z]_{(k)}\{d\} \tag{19}$$

3.2. Strain Field

From the infinitesimal strain tensor definition in equation (3), the nonzero strains associated with the assumed FSDT displacement field for an arbitrary k-layer, with $k = \{c,t,b\}$, are written as follows,

$$\begin{aligned} \varepsilon_{xx}^{(k)} &= u_{0_{(k)},x} + (z-\bar{z}_k)\theta_{x_{(k)},x} \\ \varepsilon_{yy}^{(k)} &= v_{0_{(k)},y} + (z-\bar{z}_k)\theta_{y_{(k)},y} \\ \gamma_{xy}^{(k)} &= u_{0_{(k)},y} + v_{0_{(k)},x} + (z-\bar{z}_k)\left(\theta_{x_{(k)},y} + \theta_{y_{(k)},x}\right) \\ \gamma_{xz}^{(k)} &= \theta_{x_{(k)}} + w_{0,x} \ , \ \ \gamma_{yz}^{(k)} = \theta_{y_{(k)}} + w_{0,y} \end{aligned} \tag{20}$$

where $\bar{z}_k$ is the transverse coordinate of the mid-plane of the k-layer in the global coordinate system.

3.3. Electric Potential

In order to obtain a piecewise linear LW description for the electric potential of three discrete layers, one could define the surface electric potentials, according to figure 1 as follows,

$$\phi_1\left(x,y,t\right) \equiv \phi\left(x,y,z=-h/2,t\right) \tag{21a}$$
$$\phi_2\left(x,y,t\right) \equiv \phi\left(x,y,z=-h_c/2,t\right) \tag{21b}$$
$$\phi_3\left(x,y,t\right) \equiv \phi\left(x,y,z=h_c/2,t\right) \tag{21c}$$
$$\phi_4\left(x,y,t\right) \equiv \phi\left(x,y,z=h/2,t\right) \tag{21d}$$

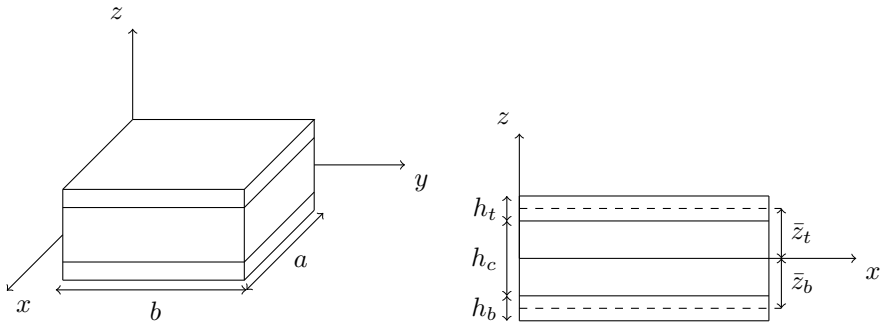

Figure 1: Piezoelectric composite plate and geometric parameters for the top, core and bottom layers.

where h the total thickness. The continuity conditions at the layer's interfaces are verified by one-dimensional linear Lagrange's functions leading to,

$$\phi_c(x,y,z,t) = f_s^c(z)\phi_3 + f_i^c(z)\phi_2 \tag{22a}$$
$$\phi_t(x,y,z,t) = f_s^t(z)\phi_4 + f_i^t(z)\phi_3 \tag{22b}$$
$$\phi_b(x,y,z,t) = f_s^b(z)\phi_2 + f_i^b(z)\phi_1 \tag{22c}$$

where for an arbitrary k-discrete layer, the transverse coordinate functions are given by:

$$f_s^{(k)}(z) = 1/2 + (z-\bar{z}_k)/h_{(k)} \tag{23a}$$
$$f_i^{(k)}(z) = 1/2 - (z-\bar{z}_k)/h_{(k)} \tag{23b}$$

Furthermore, the quadratic z-expansion of the electric potential is accomplished through the introduction of the mid-plane's potentials associated to the three discrete layers defined as shown:

$$\phi_5(x,y,t) \equiv \phi(x,y,z=\bar{z}_b,t) \tag{24a}$$
$$\phi_6(x,y,t) \equiv \phi(x,y,z=0,t) \tag{24b}$$
$$\phi_7(x,y,t) \equiv \phi(x,y,z=\bar{z}_t,t) \tag{24c}$$

The continuity conditions at the interfaces are verified by quadratic Lagrange's functions leading to,

$$\phi_c(x,y,z,t) = g_s^c(z)\phi_3 + g_i^c(z)\phi_2 + g_m^c(z)\phi_6 \tag{25a}$$
$$\phi_t(x,y,z,t) = g_s^t(z)\phi_4 + g_i^t(z)\phi_3 + g_m^t(z)\phi_7 \tag{25b}$$
$$\phi_b(x,y,z,t) = g_s^b(z)\phi_2 + g_i^b(z)\phi_1 + g_m^b(z)\phi_5 \tag{25c}$$

where for an arbitrary k-discrete layer, the transverse functions are given by:

$$g_s^{(k)}(z) = 2\left[(z-\bar{z}_k)/h_{(k)}\right]^2 + (z-\bar{z}_k)/h_{(k)} \tag{26a}$$
$$g_i^{(k)}(z) = 2\left[(z-\bar{z}_k)/h_{(k)}\right]^2 - (z-\bar{z}_k)/h_{(k)} \tag{26b}$$
$$g_m^{(k)}(z) = 1 - 4\left[(z-\bar{z}_k)/h_{(k)}\right]^2 \tag{26c}$$

The seven electric potential unknowns of the quadratic z-expansion, are ordained in the electric degrees of freedom vector $\{\varphi\}$ as follows,

$$\{\varphi\} = \{\phi_1\ \phi_2\ \phi_3\ \phi_4\ \phi_5\ \phi_6\ \phi_7\}^T \tag{27}$$

while for the linear z-expansion, only the first four variables are used.

3.4. Electric Field

The electric field for each discrete layer, assuming both linear and quadratic z-expansions of the electric potential, is derived from the field-potential relation in equation (4). For an arbitrary k-layer, the linear electric potential in equation (22) leads to the following electric field components:

$$E_x^{(k)} = -f_s^{(k)}\phi_{s,x}^{(k)} - f_i^{(k)}\phi_{i,x}^{(k)} \tag{28a}$$
$$E_y^{(k)} = -f_s^{(k)}\phi_{s,y}^{(k)} - f_i^{(k)}\phi_{i,y}^{(k)} \tag{28b}$$
$$E_z^{(k)} = (\phi_i^{(k)} - \phi_s^{(k)})/h_{(k)} \tag{28c}$$

For the quadratic z-expansion in equation (25), the associated electric field of the k-discrete layer holds:

$$E_x^{(k)} = -g_s^{(k)}\phi_{s,x}^{(k)} - g_i^{(k)}\phi_{i,x}^{(k)} - g_m^{(k)}\phi_{m,x}^{(k)} \tag{29a}$$
$$E_y^{(k)} = -g_s^{(k)}\phi_{s,y}^{(k)} - g_i^{(k)}\phi_{i,y}^{(k)} - g_m^{(k)}\phi_{m,y}^{(k)} \tag{29b}$$
$$E_z^{(k)} = -g_{s,z}^{(k)}\phi_s^{(k)} - g_{i,z}^{(k)}\phi_i^{(k)} - g_{m,z}^{(k)}\phi_m^{(k)} \tag{29c}$$

where $\phi_s^{(k)}$, $\phi_i^{(k)}$ and $\phi_m^{(k)}$ are the k-layer's potentials for the top, bottom and mid surfaces, respectively.

4. Finite Element Formulation

For both linear and quadratic z-expansions of the electric potential used in UEL1 and UEL2 models, respectively, the finite element approximation is achieved using the quadratic serendipity eight node interpolation functions (Reddy [3]), for the mechanical and electrical DOFs in equations (18) and (27), respectively. A generic matrix form for the element DOFs vectors $\{d\}^{(e)}$ and $\{\varphi\}^{(e)}$ can be achieved defining the matrices $[N]$ and $[N_\phi]$, containing the interpolation functions as shown,

$$\{d\}^{(e)} = [N]\{a\}^{(e)},\quad \{a\}^{(e)} = \{\{d\}_1^{(e)^T}...\{d\}_8^{(e)^T}\}^T \tag{30}$$
$$\{\varphi\}^{(e)} = [N_\phi]\{\bar{\varphi}\}^{(e)},\quad \{\bar{\varphi}\}^{(e)} = \{\{\varphi\}_1^{(e)^T}...\{\varphi\}_8^{(e)^T}\}^T \tag{31}$$

Moreover, for each k-layer, with $k = \{t, c, b\}$, the relation between the strain vector and the electric field components to the nodal mechanical and electrical DOFs, respectively, is achieved through,

$$\{\varepsilon\}_{(k)} = [S]_{(k)}[B]_{(k)}\{a\} \tag{32a}$$

$$\{E\}_{(k)} = -[S_\phi]_{(k)}[B_\phi]_{(k)}\{\bar{\varphi}\} \tag{32b}$$

where $[S]_{(k)}$ and $[S_\phi]_{(k)}$ are the strain transformation matrix and electric field transformation matrix, respectively, which are dependent on the transverse coordinate according to equation (20) for the strains and to equations (28) and (29) for the electric field. The strain matrices $[B]_{(k)}$ and electric field ones $[B_\phi]_{(k)}$ are dependent on the interpolation functions and their derivatives in order to relate the secondary variables to the nodal DOFs.

4.1. Element Matrices

The Hamilton's principle is used to derive the equations of motion for the plate following,

$$\delta \int_{t_1}^{t_2} T - U - W dt = 0 \tag{33}$$

where δ is the variational operator and according to Benjeddou [5], the kinetic energy T, the electromechanical energy U and the work done by distributed loads W for the present model are given by:

$$T = \sum_{k=c,t,b} \frac{1}{2} \int_{\Omega_{(k)}} \rho_{(k)} \{\dot{u}\}^T_{(k)} \{\dot{u}\}_{(k)} d\Omega_{(k)} \tag{34a}$$

$$U = \sum_{k=c,t,b} \frac{1}{2} \int_{\Omega_{(k)}} \{\varepsilon\}^T_{(k)} \{\sigma\}_{(k)} - \{E\}^T_{(k)} \{D\}_{(k)} d\Omega_{(k)} \tag{34b}$$

$$W = \sum_{k=c,t,b} \int_{S_{(k)}} \{u\}^T_{(k)} \{f_s\}_{(k)} \, dS_{(k)} \tag{34c}$$

where $\rho_{(k)}$ is the density of the k-layer, $\{\dot{u}\}_{(k)}$ the time derivative of the displacements and $\{f_s\}_{(k)}$ the distributed load vector.

Recalling the displacement-DOFs relation in equations (30) and (31), the constitutive equation (9), as well as the strain-DOFs and electric field-DOFs relations in equation (32) and following the energy principle at stationary conditions, one obtains the element equilibrium equations as follows,

$$\begin{aligned} [M_{uu}]^{(e)} \{\ddot{a}\} + [K_{uu}]^{(e)} \{a\} + [K_{u\phi}]^{(e)} \{\bar{\varphi}\} &= \{F_u\}^{(e)} \\ [K_{\phi u}]^{(e)} \{a\} + [K_{\phi\phi}]^{(e)} \{\bar{\varphi}\} &= \{0\} \end{aligned} \tag{35}$$

where $\{\ddot{a}\}$ and $\{a\}$ are the mechanical nodal DOFs and their second time derivatives, respectively, as well as $\{\bar{\varphi}\}$ the electric potential nodal DOFs. From the point of view of the UEL subroutine, the loads are applied through very soft plate elements available in Abaqus. Hence, the element mechanical load vector $\{F_u\}^{(e)}$ is not presented for brevity.

The element sub-matrices, particularly, $[M_{uu}]^{(e)}$ the mass matrix, $[K_{uu}]^{(e)}$ the elastic stiffness matrix, $[K_{u\phi}]^{(e)} = [K_{\phi u}]^{(e)^T}$ the electromechanical coupling stiffness matrices and $[K_{\phi\phi}]^{(e)}$ the dielectric stiffness matrix are given by:

$$[M_{uu}]^{(e)} = \sum_{k=c,t,b} \int_{-1}^{1} \int_{-1}^{1} \rho_{(k)} [N]^T [P]_{(k)} [N] \mathcal{J} d\xi d\eta \tag{36}$$

$$[K_{uu}]^{(e)} = \sum_{k=c,t,b} \int_{-1}^{1} \int_{-1}^{1} [B]^T_{(k)} [\hat{Q}]_{(k)} [B]_{(k)} \mathcal{J} d\xi d\eta \tag{37}$$

$$[K_{u\phi}]^{(e)} = \sum_{k=c,t,b} \int_{-1}^{1} \int_{-1}^{1} [B]^T_{(k)} [\hat{e}]_{(k)} [B_\phi]_{(k)} \mathcal{J} d\xi d\eta \tag{38}$$

$$[K_{\phi\phi}]^{(e)} = -\sum_{k=c,t,b} \int_{-1}^{1} \int_{-1}^{1} [B_\phi]^T_{(k)} [\hat{\epsilon}]_{(k)} [B_\phi]_{(k)} \mathcal{J} d\xi d\eta \tag{39}$$

where $\mathcal{J}$ the determinant of the Jacobian matrix of the transformation between the element Ω_e coordinates and the master element $\hat{\Omega}$ ones, needed to numerically evaluate the integrals through Gauss quadrature, with reduced integration for the shear terms, where a unitary shear correction factor is used, as suggested by Birman et al. [6] for sandwich structures. Hence, in order to perform exact integration, 2×2 Gauss points are used to evaluate equation (37) and 3×3 for equations (36), (38) and (39).

The $[P]_{(k)}$ matrices, for $k = \{c, t, b\}$, in equation (36) are defined as shown,

$$[P]_{(k)} = \int_{z^{inf}_{(k)}}^{z^{sup}_{(k)}} [Z]^T_{(k)} [Z]_{(k)} \, dz_k \tag{40}$$

where $z^{inf}_{(k)} = -h_{(k)}/2$ and $z^{sup}_{(k)} = h_{(k)}/2$.

Moreover, the generalized constitutive matrices $[\hat{Q}]_{(k)}$, $[\hat{e}]_{(k)}$ and $[\hat{\epsilon}]_{(k)}$ in equations (37) to (39) are obtained following the integration along the layer's thickness direction as follows:

$$[\hat{Q}]_{(k)} = \int_{z^{inf}_{(k)}}^{z^{sup}_{(k)}} [S]^T_{(k)} \left[\bar{Q}\right]_{(k)} [S]_{(k)} \, dz_k \tag{41a}$$

$$[\hat{e}]_{(k)} = \int_{z^{inf}_{(k)}}^{z^{sup}_{(k)}} [S]^T_{(k)} [\bar{e}]_{(k)} [S_\phi]_{(k)} \, dz_k \tag{41b}$$

$$[\hat{\epsilon}]_{(k)} = \int_{z^{inf}_{(k)}}^{z^{sup}_{(k)}} [S_\phi]^T_{(k)} [\bar{\epsilon}]_{(k)} [S_\phi]_{(k)} \, dz_k \tag{41c}$$

4.2. Post-Processing

According to Barlow [7], the optimal points to compute the strains, and consequently the stresses from the constitutive equation (9), coincide with the reduced integration points, i.e., the 2×2 Gauss points used in the present models. Hence, the same

points are used to compute the electric displacements, following local extrapolation for the desired location.

Since the present FSDT models assume constant transverse shear stresses, one way to possibly improve the determination of these stresses, according to Reddy [3], is based on the integration of the equilibrium equations (1) for static conditions, on the transverse direction at the Barlow's points, for each k-layer, where the quadratic shear stresses are equipped with interlaminar continuity conditions at the interfaces between adjacent layers and stress free conditions at both top and bottom surfaces.

4.3. Abaqus User-Element Implementation

Abaqus UEL subroutine translates all the developed theories and definitions in Fortran programming language. The UEL subroutine is called by Abaqus for every element within a mesh defined in the input file. According to the input file, Abaqus sends to the UEL subroutine the nodal coordinates and for each element computes the mass and stiffness matrices according to equations (36) to (39), that will be later assembled in order to obtain the overall equilibrium equations. Furthermore, this subroutine avoids the user to program the element force vector in the subroutine, using a soft dummy elements attached to the UEL mesh in the input file.

After assembling all elements, Abaqus solves the desired problem taking into account boundary conditions and loads as defined in the input file. Consequently, the solution vector containing the nodal DOFs is generated as an output. After this, Abaqus recalls the UEL subroutine for each element, adding the solution vector as an input to the UEL block, allowing post-processing procedures to be programmed. The results of interest are printed in a *.log* text file generated by Abaqus.

5. Static Analysis

The developed UEL models are compared with exact solutions available for the cases of simply-supported plates, where the top surface is subjected to an applied bi-sinusoidal distributed transverse load $q(x, y)$, as well as for the case where the same surface have instead of a load, an applied bi-sinusoidal electric potential $\hat{\phi}(x, y)$, which are given as follows:

$$q(x, y) = q_0 \sin(\pi x/a) \sin(\pi y/b) \tag{42}$$

$$\hat{\phi}(x, y) = \phi_0 \sin(\pi x/a) \sin(\pi y/b) \tag{43}$$

where for numerical applications $q_0 = 1$ N/m^2 and $\phi_0 = 1$ V. In the applied load case both plate's top and bottom surfaces are grounded, while in the applied potential case, only the bottom surface is grounded.

5.1. Problem Description

Two symmetric stacking schemes are considered as test cases, based on some numerical applications reported in Moleiro et al. [2], where a multilayered graphite-epoxy core made of three unidirectional fiber reinforced composite layers is bonded in both faces with piezoelectric layers as follows: Case 1- Transversely isotropic piezoceramic PZT-4 face layers [PZT-4/0°/90°/0°/PZT-4]; Case 2- Orthotropic piezoelectric polymer PVDF face layers of 0° [PVDF/90°/0°/90°/PVDF]. The associated engineering constants, piezoelectric coefficients and relative dielectric constants are listed in table 1. Square plates ($a = b$) are considered with fixed total thickness $h = 0.01$ m. Each piezoelectric layer has $h/10$ of thickness, while the multilayered composite core has $8h/10$ with equal thickness composite layers. The side dimension a is determined by the plate's aspect ratio $a/h = 100,\ 20,\ 10$ or 4.

Table 1: Material properties from Moleiro et al. [2].

Properties	G-E	PZT-4	PVDF
E_1 (GPa)	132.28	81.3	237.0
E_2 (GPa)	10.756	81.3	23.2
E_3 (GPa)	10.756	64.5	10.5
G_{12} (GPa)	5.654	30.6	6.43
G_{13} (GPa)	5.654	25.6	4.40
G_{23} (GPa)	3.606	25.6	2.15
ν_{12}	0.24	0.33	0.154
ν_{13}	0.24	0.43	0.178
ν_{23}	0.49	0.43	0.177
e_{15} (C/m^2)	0	12.72	-0.01
e_{24} (C/m^2)	0	12.72	-0.01
e_{31} (C/m^2)	0	-5.20	-0.13
e_{32} (C/m^2)	0	-5.20	-0.14
e_{33} (C/m^2)	0	15.08	-0.28
ϵ_{11}/ϵ_0 *	3.5	1475	12.50
ϵ_{22}/ϵ_0 *	3.0	1475	11.98
ϵ_{33}/ϵ_0 *	3.0	1300	11.98

*$\epsilon_0 = 8.85 \times 10^{-12}$ F/m (vacuum constant)

The simply-supported boundary conditions for the three discrete layers imply the following conditions:

$$u_{0_{(k)}} = w_0 = \theta_{x_{(k)}} = \phi_i = 0 \ \text{ at } y = 0, a \tag{44a}$$

$$v_{0_{(k)}} = w_0 = \theta_{y_{(k)}} = \phi_i = 0 \ \text{ at } x = 0, a \tag{44b}$$

with $k = \{t, c, b\}$ and $i = \{1, 2, 3, 4\}$ for UEL1, while $i = \{1, 2, ..., 7\}$ for UEL2.

It should be enhanced that all results are given at absolute maximum in-plane locations, using SI units: $[u, z]$ = m, $[\phi]$ = V, $[\sigma]$ = Pa, and $[D]$ = C/m^2. Moreover, in the presentation of the predicted transverse shear stresses by the developed models, the suffix (C) stands for constitutively derived stresses, while the suffix (E) stands for the equilibrium derived ones. A mesh with 30×30 elements is used for both static and dynamic analysis, for all plate's dimensions, in order to ensure converged solutions.

5.2. Thin and Moderately Thick Plates Results

The predictive capabilities of the developed UEL models in static response, for thin and moderately thick piezoelectric composite plates, under applied load or potential, is demonstrated by the resemblance between the UEL static analysis results and the exact ones, in terms of displacements, electric potential and in-plane stresses shown in tables 2 and 3, particularly for the Case 1 as shown in figures 2 and 3. However, due to the assumption of constant transverse shear strains, in each discrete layer, some shortcomings are detected, particularly in the applied load case. In fact, for the applied load case, the FSDT assumptions lead to an inaccurate description of the in-plane electric displacements within the piezoelectric layers, since these variables are dependent on the shear strains, which are assumed to be constant in each discrete layer. Also, even the quadratic z-expansion for the electric potential appears to be slightly inappropriate for a sufficiently accurate evaluation of the transverse electric displacements for the piezoelectric layers of moderately thick plates, under applied load.

The aforementioned discrepancies become more pronounced for moderately thick plates of Case 2, where the transversely softer piezoelectric polymer PVDF undergoes in larger normal compressibility effects, where the transverse normal strains and transverse shear strains play an important role. Therefore, in the applied load case, a poorest performance of both UEL models is achieved in the assessment of the in-plane displacements, in-plane stresses as well as in the electric potential distribution and consequently on the electric displacements, comparatively to Case 1, that concerns the piezoceramic PZT-4. Likewise, for the applied potential case, this transversely softer behaviour of PVDF produces considerable through-thickness variations of transverse displacement, that can not be taken into account in the present FSDT based models, with negligible transverse normal strains.

On the other hand, the UEL results for the plates with the piezoceramic PZT-4 in Case 1, under applied potential, almost match the exact solutions for thin and moderately thick plates, including in-plane stresses and electric displacements. In this case, the hypothesis of constant transverse displacement is far more accurate than for the PVDF case, being the transverse displacements of the UEL2 model the most precise comparatively to UEL1, as can be seen in figure 3. This result suggests that the present electro-elastic elements are more suitable to be used in the analysis of sensors or actuators made of harder piezoelectric materials with lower normal compressibility and transverse shearing effects.

Ultimately, for both applied load and potential cases, the displacements and the electric potential are almost independent on the linear or quadratic z-expansion used for the electric potential, being both good approximations to the exact solutions for thin and moderately thick plates. However, the UEL2 displacements and electric potential are slightly more precise than UEL1 within the piezoelectric layers, for both monitoring and actuation modes, leading to improved predictions of in-plane stresses and electric displacements.

Regarding the evaluation of the transverse shear stresses, figure 4 shows that the integration of the equilibrium equations provides a better description of these stresses than the constitutive approach, fulfilling the interlaminar continuity conditions and the stress free conditions for both top and bottom plate surfaces. Although both methods fail on an accurate determination of transverse shear stresses with respect to the exact solutions, both constitutively and equilibrium derived stresses give an idea of the stress state in each layer, where the second ones offers an exact distribution except for a correction factor, dependent on the loading, dimensions and material properties.

6. Free Vibration Analysis

The first twelve vibration frequencies ω_{mn} and associated modes (m, n) are determined for the same stacking sequences used in static analysis (Section 5.1) with simply-supported conditions defined in equation (44). Additionally, from Moleiro et al. [8], the grounded homogeneous potential conditions on both plate's surfaces are used, i.e.,

$$\phi(x, y, z = h/2) = \phi(x, y, z = -h/2) = 0 \qquad (45)$$

since they provide lower vibration frequencies when compared to other sets of possible electric boundary conditions. For comparison proposes, the same unitary density is used for both piezoelectric and composite materials, i.e., $\rho = 1$ kg/m^3.

Table 4 shows the first twelve vibration frequencies and associated modes for moderately thick and thick plates with $a/h = 10$ and 4, respectively, for both Case 1 and Case 2, using both linear and quadratic z-expansions of the electric potential (UEL1 and UEL2), including the relative error to the exact solution reported by Moleiro et al. [2]. From the comparison of the results predicted by the UEL models and the exact solutions one can conclude that both UEL models predict the first twelve vibration modes and associated frequencies, for moderately thick and thick plates in good resemblance to the exact ones.

One could see that among the first twelve vibration frequencies, some special modes, with null transverse displacement, known as membrane modes, in the form of $(m, 0)$ and $(0, n)$ emerge between the flexural modes, where the elastic and elec-

Table 2: Results for Case 1 and Case 2, with $a/h = 100$ and 20, under applied bi-sinusoidal load.

		Case 1					Case 2				
	a/h	Exact	UEL1	$\delta_1(\%)$	UEL2	$\delta_2(\%)$	Exact	UEL1	$\delta_1(\%)$	UEL2	$\delta_2(\%)$
$u\left(0,\frac{a}{2},\frac{h}{2}\right)\times 10^{12}$	100	-6492.82	-6500.18	0.11	-6497.32	0.07	-8364.63	-8366.16	0.02	-8366.15	0.02
	20	-51.970	-52.118	0.28	-52.093	0.24	-66.628	-66.580	-0.07	-66.580	-0.07
$w\left(\frac{a}{2},\frac{a}{2},\frac{h}{2}\right)\times 10^{11}$	100	41457.67	41496.31	0.09	41478.06	0.05	53397.96	53402.20	0.01	53402.09	0.01
	20	71.066	70.933	-0.19	70.900	-0.23	90.708	90.392	-0.35	90.392	-0.35
$\phi\left(\frac{a}{2},\frac{a}{2},\frac{9h}{20}\right)\times 10^{3}$	100	21.432	20.105	-6.19	21.216	-1.01	17.944	16.856	-6.07	17.793	-0.84
	20	0.858	0.807	-5.90	0.855	-0.39	0.829	0.677	-18.37	0.716	-13.68
$\sigma_{xx}\left(\frac{a}{2},\frac{a}{2},\frac{h}{2}\right)$	100	3145.34	3084.31	-1.94	3149.92	0.15	6339.58	6351.84	0.19	6352.10	0.20
	20	127.01	124.08	-2.31	126.88	-0.10	252.79	252.84	0.02	252.85	0.02
$D_x\left(0,\frac{a}{2},\frac{h}{2}\right)\times 10^{12}$	100	0.00	2790.69	-	2792.06	-	0.00	-22.29	-	-22.29	-
	20	0.00	559.98	-	560.27	-	0.00	-4.43	-	-4.43	-
$D_z\left(\frac{a}{2},\frac{a}{2},\frac{h}{2}\right)\times 10^{12}$	100	12.026	-61000	-	12.283	2.14	-0.92	-425.99	-	-0.21	-78
	20	12.182	-2604	-	11.280	-7.40	-0.93	-17.83	-	-0.21	-77

$\delta_i = (x_{\text{UEL}i} - x_{\text{Exact}}) \times 100/x_{\text{Exact}}$

Table 3: Results for Case 1 and Case 2, with $a/h = 100$ and 20, under applied bi-sinusoidal potential.

		Case 1					Case 2				
	a/h	Exact	UEL1	$\delta_1(\%)$	UEL2	$\delta_2(\%)$	Exact	UEL1	$\delta_1(\%)$	UEL2	$\delta_2(\%)$
$u\left(0,\frac{a}{2},\frac{h}{2}\right)\times 10^{12}$	100	-2.949	-2.861	-2.96	-2.864	-2.86	-1.188	-1.182	-0.49	-1.182	-0.49
	20	-6.845	-6.800	-0.66	-6.815	-0.45	-0.235	-0.225	-4.11	-0.226	-4.07
$w\left(\frac{a}{2},\frac{a}{2},\frac{h}{2}\right)\times 10^{11}$	100	-1.203	-1.224	1.74	-1.205	0.23	0.092	0.020	-78	0.021	-77
	20	-1.218	-1.232	1.13	-1.213	-0.45	0.093	0.021	-78	0.021	-78
$\phi\left(\frac{a}{2},\frac{a}{2},0\right)$	100	0.4999	0.5000	0.02	0.4999	0.00	0.4999	0.5000	0.02	0.4999	0.00
	20	0.4977	0.4999	0.43	0.4977	0.00	0.4975	0.4996	0.43	0.4975	0.00
$\sigma_{xx}\left(\frac{a}{2},\frac{a}{2},\frac{h}{2}\right)$	100	-2.521	-2.360	-6.41	-2.489	-1.27	-1.098	-1.096	-0.15	-1.097	-0.09
	20	2.258	5.633	150	2.391	5.1	-1.163	-1.177	1.24	-1.194	2.65
$D_x\left(0,\frac{a}{2},\frac{h}{2}\right)\times 10^{8}$	100	-6.088	-6.097	0.15	-6.097	0.15	-0.03478	-0.03482	0.13	-0.03482	0.13
	20	-30.442	-30.484	0.14	-30.484	0.14	-0.1739	-0.1741	0.13	-0.1741	0.13
$D_z\left(\frac{a}{2},\frac{a}{2},\frac{h}{2}\right)\times 10^{8}$	100	-0.370	-0.359	-3.10	-0.371	0.14	-0.3140	-0.3144	0.10	-0.3145	0.14
	20	-1.292	-0.994	-23.07	-1.294	0.15	-0.323	-0.320	-0.68	-0.323	0.13

$\delta_i = (x_{\text{UEL}i} - x_{\text{Exact}}) \times 100/x_{\text{Exact}}$

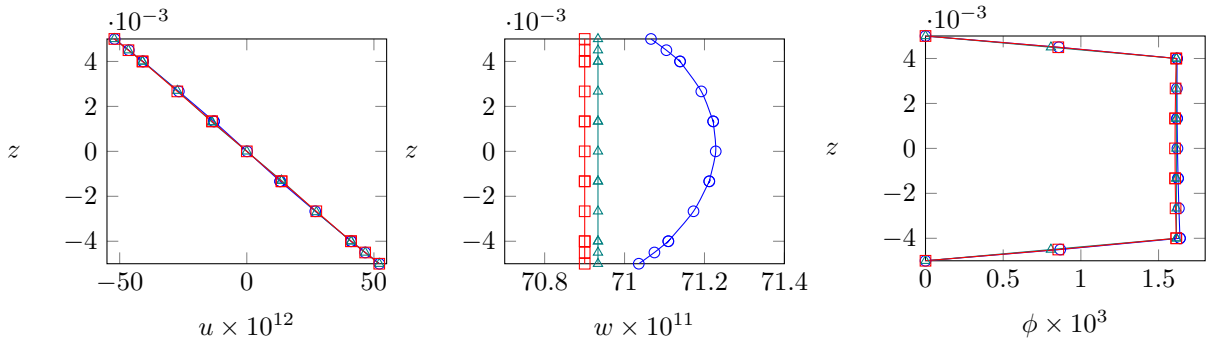

Figure 2: In-plane displacement $u\,(0, a/2, z)$, transverse displacement $w\,(a/2, a/2, z)$ and electric potential $\phi\,(a/2, a/2, z)$ for Case 1, with $a/h = 20$, under applied bi-sinusoidal load: Exact (—○—), UEL1 (—△—) and UEL2 (—□—).

tric domains decoupled and therefore the UEL models coincide. These special modes are more prompt to occur as the the side-to-thickness ratio decreases and only exhibit harmonic motion on the in-plane displacements, opposing to the flexural modes.

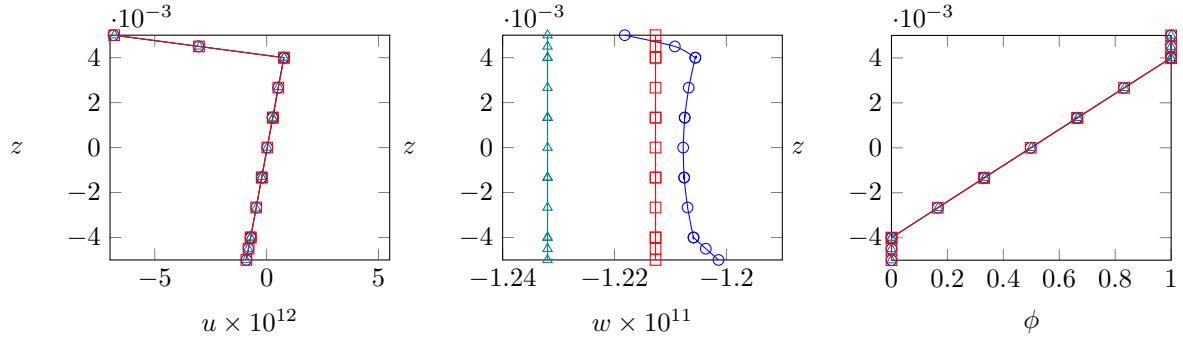

Figure 3: In-plane displacement $u\,(0, a/2, z)$, transverse displacement $w\,(a/2, a/2, z)$ and electric potential $\phi\,(a/2, a/2, z)$ for Case 1, with $a/h = 20$, under applied bi-sinusoidal potential: Exact (—○—), UEL1 (—△—) and UEL2 (—□—).

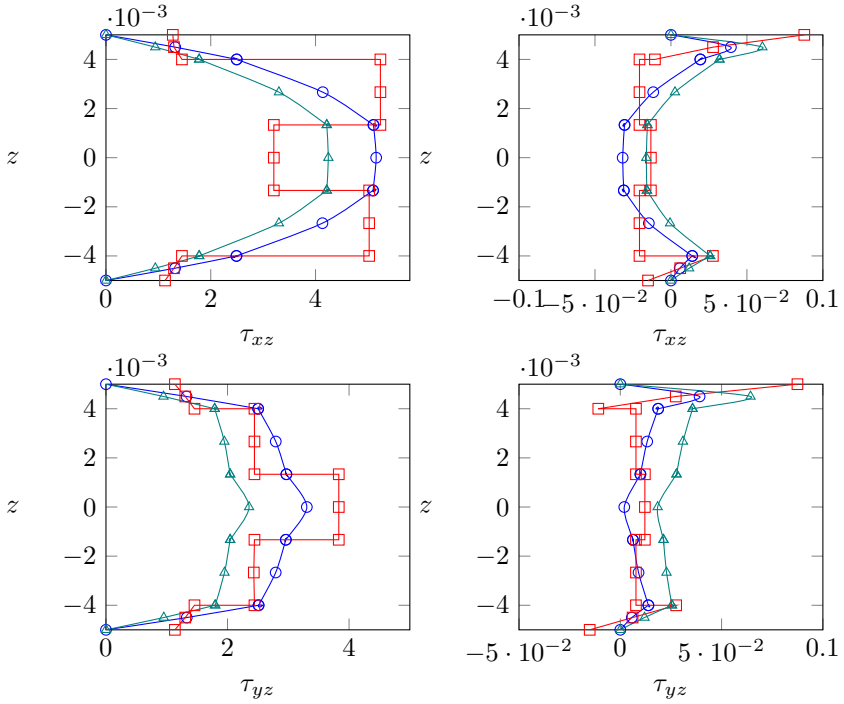

Figure 4: Shear stresses $\tau_{xz}(0, a/2, z)$ and $\tau_{yz}(a/2, 0, z)$ for Case 1, with $a/h = 20$, under applied load (on the left) and applied potential (on the right): Exact (—○—), UEL2(C) (—□—), UEL2(E) (—△—).

Furthermore, in Case 1 both UEL models conduct to very similar vibration frequencies, while in Case 2 the models are coincident, due to a weaker electromechanical coupling when compared to Case 1, i.e., lower piezoelectric coefficients (table 1), and consequent insensitivity to the linear or quadratic z-expansions of the electric potential.

7. Conclusions

The present work regards the development, implementation and validation with exact solutions, of two LW electro-elastic UEL models in Abaqus, completing the lack of piezoelectric plate elements in the software's library. In fact, the present work and achieved results represent a complement to the literature, particularly by implementing an Abaqus UEL subroutine to access a comprehensive comparison, relatively to the exact solutions, of the performance of two discrete LW classical electro-elastic plate elements with a piecewise linear displacement field combined with a linear or quadratic z-expansions of the electric potential, in both static and free vibration analysis, for two different piezoelectric materials considering the case of thin, moderately thick and thick plates.

To sum up, the conformity between the UEL results and the exact solutions in the test cases, suggests the capability of the developed elements to perform static analysis, in monitoring modes and specially in actuation modes, of thin and mod-

Table 4: First twelve natural frequencies ω_{mn} (10^5rad/s) of Case 1 and Case 2, with $a/h = 10$ and 4.

	Case 1						Case 2			
a/h	(m,n)	Exact	UEL1	$\delta_1(\%)$	UEL2	$\delta_2(\%)$	(m,n)	Exact	UEL*	$\delta(\%)$
10	(1,1)	13.526	13.647	0.9	13.651	0.9	(1,1)	12.113	12.234	1.0
	(1,2)	27.822	27.963	0.5	27.975	0.5	(0,1)	23.944	23.945	0.0
	(2,1)	30.949	31.831	2.9	31.841	2.9	(1,0)	23.944	23.945	0.0
	(1,0)	32.365	32.410	0.1	32.410	0.1	(1,2)	26.010	27.098	4.2
	(0,1)	32.380	32.410	0.1	32.410	0.1	(2,1)	29.515	29.831	1.1
	(2,2)	41.578	42.321	1.8	42.340	1.8	(2,2)	37.899	38.874	2.6
	(1,3)	47.104	47.323	0.5	47.349	0.5	(1,3)	44.470	47.311	6.4
	(3,1)	51.608	53.541	3.7	53.563	3.8	(0,2)	47.888	47.890	0.0
	(2,3)	57.615	58.297	1.2	58.331	1.2	(2,0)	47.888	47.890	0.0
	(3,2)	59.845	61.500	2.8	61.535	2.8	(3,1)	50.294	50.995	1.4
	(2,0)	64.462	64.811	0.5	64.811	0.5	(2,3)	52.604	55.169	4.9
	(0,2)	64.579	64.811	0.4	64.811	0.4	(3,2)	55.832	56.959	2.0
4	(1,1)	57.074	58.176	1.9	58.208	2.0	(1,1)	52.241	53.895	3.2
	(1,0)	80.330	81.008	0.8	81.008	0.8	(0,1)	59.859	59.862	0.0
	(0,1)	80.555	81.008	0.6	81.008	0.6	(1,0)	59.859	59.862	0.0
	(1,2)	101.421	102.451	1.0	102.568	1.1	(1,2)	93.081	98.837	6.2
	(2,1)	105.244	107.916	2.5	108.030	2.6	(2,1)	98.627	100.728	2.1
	(2,2)	136.604	138.770	1.6	138.992	1.7	(0,2)	119.712	119.721	0.0
	(1,3)	152.192	153.589	0.9	153.902	1.1	(2,0)	119.713	119.721	0.0
	(2,0)	156.766	161.909	3.3	161.909	3.3	(2,2)	125.243	130.479	4.2
	(0,2)	158.412	161.909	2.2	161.909	2.2	(1,3)	141.135	149.389	5.8
	(3,1)	159.576	162.070	1.6	162.367	1.7	(3,1)	148.353	151.204	1.9
	(2,3)	178.693	180.857	1.2	181.303	1.5	(2,3)	164.142	171.993	4.8
	(3,2)	183.055	185.395	1.3	185.828	1.5	(3,2)	167.209	172.439	3.1

$\delta_i(\%) = (\omega_{\text{UEL}i} - \omega_{\text{Exact}}) \times 100/\omega_{\text{Exact}}$, *UEL1≡UEL2

erately thick piezoelectric multilayered composite plates, as well as to perform free vibration analysis to access the vibration modes and associated frequencies. However, some inherent limitations of the FSDT displacement field must be kept in mind, with an overall advantage in static analysis of the quadratic z-expansion of the electric potential as the side-to-thickness ratio decreases.

These models represent a breakthrough for preliminary modelling and analysis of smart piezoelectric composite plates, since the developed finite element models can be easily implement for other flat geometries, with different boundary conditions and also with less computational effort than common three-dimensional elements. Furthermore, due to the highlighted level of accuracy in free vibration analysis, both finite element models are suitable to be used in optimization processes, as well as in active vibration control using feed-back control laws.

References

[1] Heyliger P.R. Exact solutions for simply supported laminated piezoelectric plates. *Journal of Applied Mechanics*, 64:299–306, 1997.

[2] Moleiro F., Mota Soares C.M., Carrera E., and Reddy J.N. Evaluation of exact electro-elastic static and free vibration solutions of multilayered plates for benchmarking: piezoelectric composite laminates and soft core sandwich plates. *Composites Part C: Open Access*, 2, 2020. doi:https://doi.org/10.1016/j.jcomc.2020.100038.

[3] Reddy J.N. *Mechanics of Laminated Composite Plates and Shells – Theory and Analysis*. Boca Raton, CRC Press, 2nd edition, 2004.

[4] Carrera E. Theories and finite elements for multilayered anisotropic, composite plates and shells. *Archives of Computational Methods in Engineering*, 9(2):87–140, 2002.

[5] Benjeddou A. Advances in piezoelectric finite element modeling of adaptive structural elements, a survey. *Computers and Structures*, 76:347–363, 2000.

[6] Birman V. and Bert C.W. On the choice of shear correction factor in sandwich structures. *Journal of Sandwich Structures and Materials*, 4:83–95, 2002.

[7] Barlow J. Optimal stress locations in finite element models. *International Journal for Numerical Methods in Engineering*, 10:243–251, 1976.

[8] Moleiro F., Araújo A.L., and Reddy J.N. Benchmark exact free vibration solutions for multilayered piezoelectric composite plates. *Composite Structures*, 182:598–605, 2017.